

Development of a Photoemission Microscopy Apparatus Using a Vacuum Ultraviolet Laser

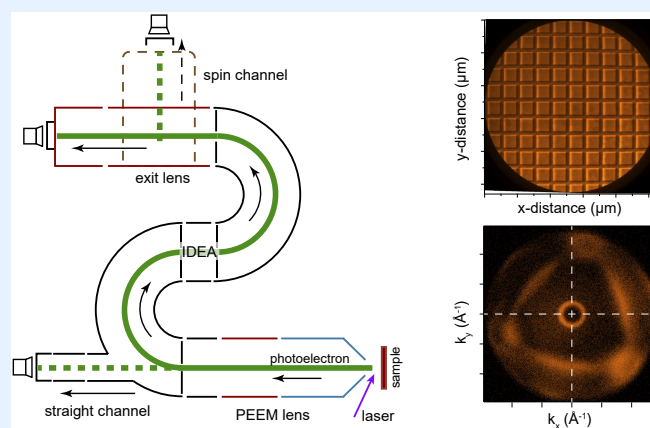
Koichiro Yaji,[†] Shunsuke Tsuda

Center for Basic Research on Materials, National Institute for Materials Science, 3-13 Sakura, Tsukuba, Ibaraki, 305-0003, Japan

[†] Corresponding author: yaji.koichiro@nims.go.jp

Received: 7 August, 2023; Accepted: 6 September, 2023; J-STAGE Advance Publication: 12 October, 2023; Published: 12 October, 2023

We report on a photoemission microscopy apparatus using a 10.9-eV laser developed at the National Institute for Materials Science (NIMS). Our spectrometer realizes photoemission spectroscopy with a high spatial resolution by combining an imaging double energy analyzer with the electronic lens system of photoelectron emission microscopy. Energy-filtered photoelectron imaging is available in both real and momentum spaces. The spatial resolution in the real space mode is ~ 30 nm. We show energy-filtered photoelectron images of a silver grid-patterned sample in real space and the band mapping of Au(111) in momentum space to demonstrate the performance of our spectrometer.



Keywords Photoemission spectroscopy; Momentum microscope; Ultraviolet laser; Electronic property

1. INTRODUCTION

Electronic states near the Fermi level play an important role in determining the electrical and magnetic properties of materials. Thus, visualization of the behavior of electrons in materials is quite useful for designing and developing functional devices. Electronic states in materials are described by three quantum numbers: energy, momentum, and spin. Angle-resolved photoemission spectroscopy (ARPES) enables us to observe the energy dispersion of the band [1]. Spin-resolved photoemission spectroscopy provides information on the spin-polarized band structure [2]. Thus, the photoemission spectroscopy of the valence band is a powerful technique for characterizing materials. ARPES has played a central role in the study of electronic states for superconductors, topological materials, low-dimensional materials, etc. [3] Furthermore, in the last decade, there has been a tremendous movement toward probing electronic states in a sub-micrometer region [4]. This is due to the demands of elucidating the local electronic states of materials for developing innovative devices. For instance, the studies of superconducting states and topological phases in novel quantum materials

require the characterization of electronic bands below the sub-micrometer region [5, 6]. Conventional photoemission spectroscopy has a spatial resolution of several tens of μm or more, making it challenging to obtain information on the local electronic states in a few-micrometer to sub-micrometer region.

In this context, the development of photoemission microscopy apparatuses for investigating the electronic state in the sub-micrometer region has recently been accelerated. Synchrotron radiation facilities are leading the development of such apparatuses: currently, the photoemission microscopy machines for analyzing the valence electrons in the several hundred-nanometer ranges are operated at several synchrotron radiation facilities [7–10]. In addition, a spatial resolution of 70 nm was achieved by core-level photoemission microscopy with an external voltage applied at BL07LSU at SPring-8, resulting in a deep understanding of the electronic structure of materials in their operating environment [11]. In these techniques, synchrotron radiation is focused using optical focusing mirrors and/or Fresnel zone plates, and the sample is scanned in the lateral direction to obtain the spatially resolved electronic state.

Recently, an imaging-type spectrometer for photoemission microscopy, which utilizes a different mechanism from the scanning type in principle, the so-called momentum microscope, has made significant progress [12–20]. This spectrometer realizes the high spatial resolution by employing the electronic lens system based on photoelectron emission microscopy (PEEM) in the lens section of the photoelectron analyzer. The photoelectrons emitted from a sample are typically accelerated to energies of 10–20 keV by the high electrostatic field between the first electronic lens of the analyzer and the sample. Thus, high spatial resolution can be achieved even in low-energy photoexcitation, such as an ultraviolet laser, not limited by the diffraction limit of the incident light. The spatial resolution of 2.6 nm has been achieved in PEEM using a 4.66-eV ($\lambda = 266$ nm) laser [21]. We note here that the spatial resolution of the PEEM is restricted by the intrinsic vibration originating from the instrument itself in most cases. Thus, this imaging-type spectrometer enables photoemission microscopy with lab-based light sources, such as a laser, a mercury (Hg) lamp, a helium (He) lamp, and an X-ray tube, without synchrotron radiation. Besides, thanks to the PEEM lens system, one can quickly switch between real-space and momentum-space measurements. These technologies are employed in Nano-ESCA [12–15] and Momentum Microscopy [16–20]. These spectrometers are capable of electronic state measurements in three measurement modes: (1) non-energy filter PEEM mode, where the magnified images of the surface can be observed, (2) energy-filtered photoelectron imaging mode in real space, where the area-selected imaging from the work function cut-off to the Fermi level cut-off energies is available, (3) energy-filtered photoelectron imaging mode in momentum space, where the band mapping in a selected area with an aperture is available. Photoemission microscopy apparatuses using Nano-ESCA or Momentum Microscopy have been developed at several synchrotron radiation facilities [14, 16, 20]. The time-resolved measurements using a pulsed laser [22, 23] and the chemical analysis using a brilliant X-ray [24] have been performed in the laboratory-based system.

In this article, we report on a photoemission microscopy apparatus using a 10.9-eV laser recently developed at the National Institute for Materials Science (NIMS). Our machine is equipped with Nano-ESCA with a state-of-the-art Imaging Double Energy Analyzer (IDEA). This allows one to obtain energy-filtered photoelectron images in real and momentum spaces. The spectrometer achieves an energy resolution of 24 meV, a special resolution of ~ 30 nm in a real space mode, and a wave number (k) resolution of 0.02 \AA^{-1} in a momentum space mode. We show the band mapping of Au(111) as a demonstration of ARPES.

II. INSTRUMENTS

A. Overview of the apparatus

Figure 1 shows an overview of the photoemission micros-

copy apparatus developed at NIMS. Our apparatus consists of three ultrahigh vacuum (UHV) chambers: an analysis chamber, an intermediate chamber, and a sample preparation chamber. These chambers are connected via UHV gate valves. The base pressure of the analysis chamber is kept below 1.5×10^{-8} Pa. The analysis chamber is equipped with a vacuum ultraviolet (VUV) laser, a He discharge lamp, and a Hg lamp as excitation light sources. The VUV laser is incident at an angle of 65° with respect to the sample surface normal. The incident plane of the VUV laser is parallel to the x - z plane. Photoelectrons are analyzed by Nano-ESCA made by Focus GmbH. The typical distance between the sample and the photoelectron analyzer is approximately 2.5 mm. The sample manipulator is driven by a stepping motor in 6 axes: x , y , z , θ_x , θ_y , and ϕ . Samples can be cooled below 20 K using liquid helium. One can access from the intermediate chamber to the analysis and sample preparation chambers using UHV transfer rods. Six samples can be stocked in the intermediate chamber. A load lock for sample entry and a UHV suitcase made by Ferrovac AG can be connected to the intermediate chamber. The sample preparation chamber is equipped with an Ar^+ sputter gun and a low-energy electron diffraction (LEED) instrument. Three ports are provided for evaporator mounting. Samples can be heated by both direct current heating and electron bombardment heating. The sample manipulators in the sample preparation chamber can be cooled with liquid nitrogen and liquid helium.

B. 10.9-eV laser

The electrons in the sample are excited by 10.9-eV (113.8 nm wavelength) photons, yielded by the 9th harmonic of a Yb fiber laser with the wavelength of 1024 nm (OXIDE UV-3), where the basic idea of the laser system has been reported in the reference [25]. The repetition rate is 50 MHz, and the pulse duration is less than 20 ps. Our laser system offers linear horizontally and vertically polarized lights and left- and right-circularly polarized lights with individually controllable half- and quarter-wave plates.

Using the high-brilliant laser provides a significant advantage in drastically improving the energy and momentum resolutions of photoemission spectroscopy [26–28]. On the other hand, the photon energy of the laser in most laser-ARPES is 6–7 eV, resulting in the observable wavenumber k below $0.6\text{--}0.8 \text{ \AA}^{-1}$. The 6–7 eV lasers are significantly helpful in the electronic structure measurements near the Γ point. In contrast, photoexcitation with a 10.9-eV laser extends the observable wavenumber to 1.3 \AA^{-1} . Thus, the electronic states from the Γ point to the edge of the first Brillouin zone for many materials are observable.

C. Photoelectron analyzer

Our Nano-ESCA comprises a PEEM lens system, IDEA, a delay line detector (DLD), and a two-dimensional (2D) imaging unit with multi-channel plates and a CMOS camera [Figure 2(a)]. The PEEM lens system allows photoelectron imaging in real (x - y) and momentum (k_x - k_y) spaces. The straight channel without IDEA provides standard PEEM

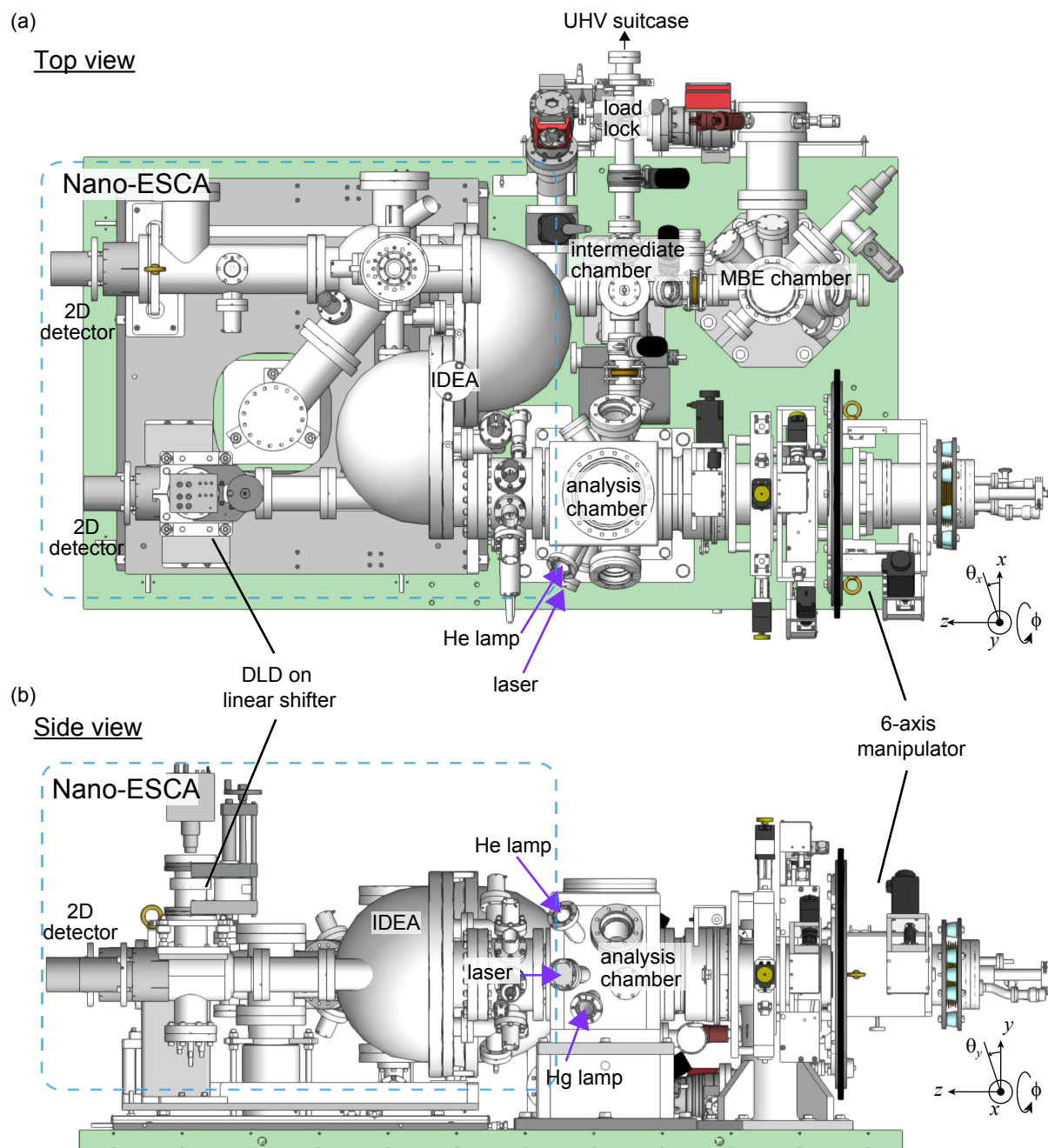


Figure 1: Overview of the apparatus. The top and side views are shown in (a) and (b), respectively.

images. The straight channel is equipped with the DLD on a linear shifter. Thus, inserting the DLD into the PEEM column realizes time-of-flight energy analysis in the straight channel. Photoemission spectroscopy using this DLD will be described elsewhere. In this article, we focus on the energy analysis with the IDEA. Photoelectrons traveling through the PEEM lens are energy-filtered by the IDEA. Here, one can select five different pass energies: 12.5, 25, 50, 100, and 200 eV, and five slit widths: 0.2, 0.5, 1, 2, and 8 mm. The spin analysis is possible by inserting a spin detector in the exit lens section of the IDEA. The maximum measurable wave number of Nano-ESCA is $k_{x,y} \sim \pm 3.0 \text{ \AA}^{-1}$.

Thus, the Nano-ESCA can simultaneously analyze the photoelectrons emitted in the range of 2π sr with photoelectron kinetic energies below ~ 34 eV. In the measurement, the magnification of the real and momentum spaces can be optimized according to the electronic state to be observed. Furthermore, a spot selector (continuously variable iris aperture) can select an area of interest down to sub-micrometers.

D. Laser spot size

The PEEM image of a silver (Ag) grid-patterned sample on a silicon (Si) substrate measured with a field of view (FoV) of $711 \mu\text{m}$ is shown in Figure 2(b). The thickness of

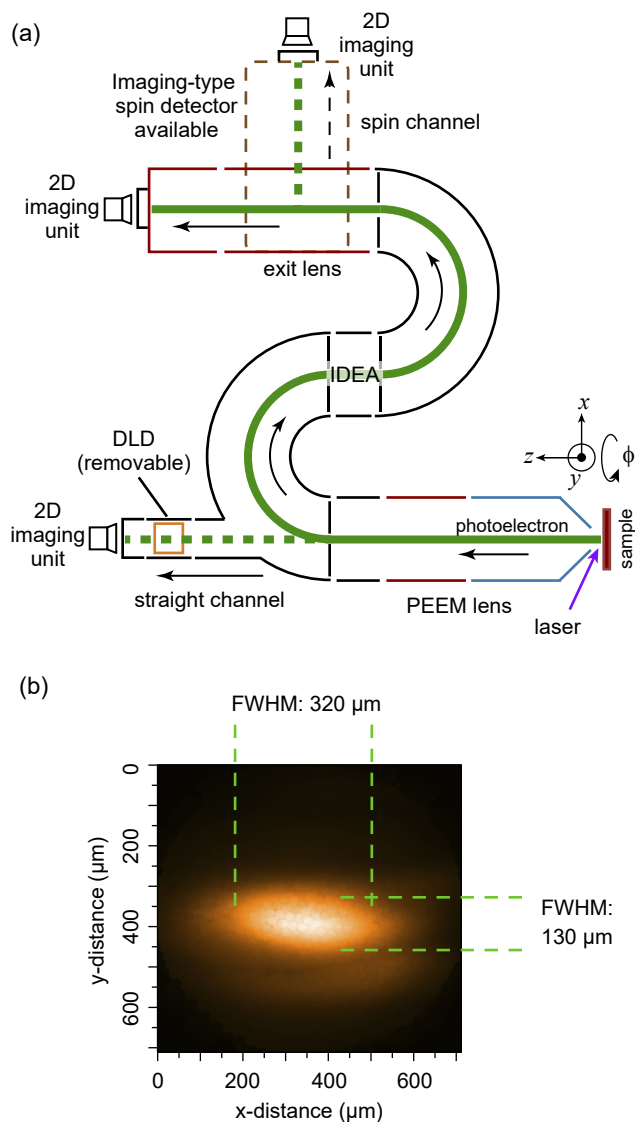


Figure 2: (a) Schematic drawing of Nano-ESCA. Bold green lines represent the photoelectron trajectory. (b) Photoelectron intensity mapping from the Ag grid-patterned sample on the Si substrate in the real space with a FoV of 711 μm . The 10.9-eV laser is used as an excitation light.

Ag is roughly 40 nm. The sample is the same as shown in Figure 3, but the grid pattern is not visible in Figure 2(b) because the grid size is much smaller than the FoV. From this photoelectron intensity mapping, the full-width half maximum (FWHM) of the laser spot on the sample is estimated to be 320 μm in the horizontal direction and 130 μm in the vertical direction. Here, the actual beam size in the horizontal direction is 140 μm since the incident angle of the laser to the sample normal is 65°. Therefore, the laser spot shape is almost circular, while the horizontal footprint on the sample is elongated due to the oblique incidence. Stray light is found 150 μm below the main spot.

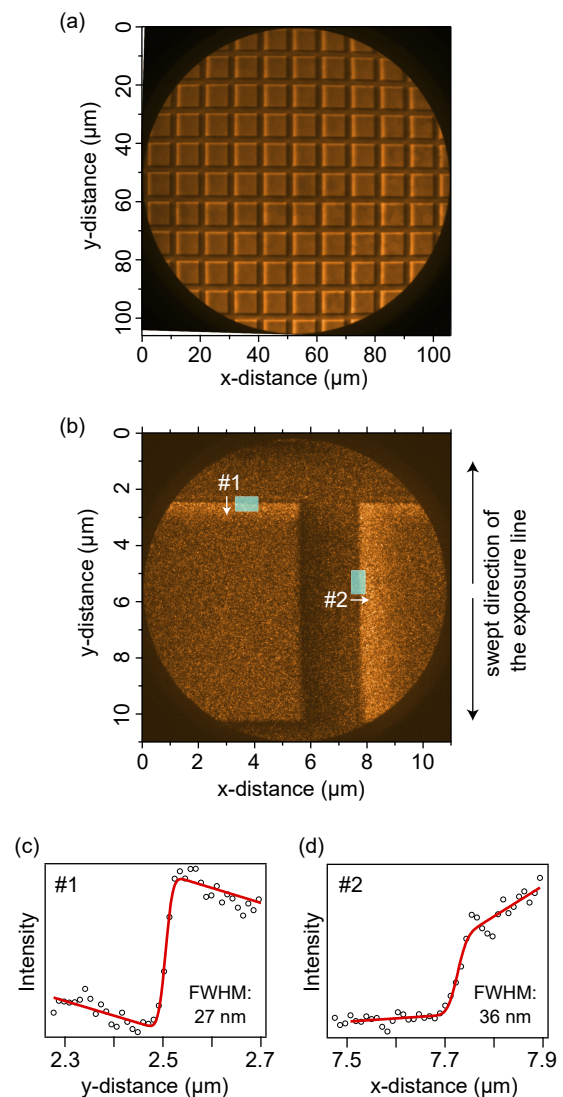


Figure 3: Photoelectron intensity mapping of the square grid pattern of Ag on the Si substrate in real space with the FoV of 104 μm (a) and 10.7 μm (b), where the photoelectron near the cut-off energy by the work function is detected. Photoelectrons were excited by the Hg lamp ($h\nu = 5.2$ eV). The exposure line of the CMOS camera is swept from the center to outward in the y-direction. (c, d) Photoelectron intensity profiles along #1 and #2 shown in (b). Each data point is obtained by the summation of the photoelectron intensity within a window given by the line widths of #1 and #2. Circle symbols represent the experimental data. Solid curves are fitting results with the step function convoluted by the Gaussian.

III. PERFORMANCE

A. Spatial resolution

Figure 3(a, b) shows a photoelectron image with 104 and 10.7 μm FoVs from the Ag grid pattern on the Si substrate, respectively. Each patch is an $8 \times 8 \mu\text{m}^2$ square separated by trenches with 2 μm widths. We used the Hg lamp as the excitation light source. We detected the photoelectrons with almost zero kinetic energy, meaning that the contrast in the

image reflects the difference in photoelectron yield resulting from the work function difference between the square patches and the trenches. The measurement was performed at room temperature. We set to the pass energy of 100 eV for IDEA. The exposure time of the CMOS camera was 10 ms.

The photoelectron intensity profiles at the edges of the square patches along #1 and #2 are shown in Figure 3(c, d), respectively. We evaluate the spatial resolution from these intensity profiles in the real space mode. The intensity profiles are fitted by a step function convoluted by a Gaussian, where linear functions with different slopes on the trench and the square patch are used as a background. Here, we defined the spatial resolution by the FWHM of the Gaussian. As a result, the spatial resolution at #1 (#2) is estimated to be 27 nm (36 nm). We find that the spatial resolution in the y -direction is 30% better than that in the x -direction. This result might be caused by the image acquisition method of the CMOS camera. The image readout of the CMOS camera adopts a rolling shutter method, where an exposure line along the x -axis with one-pixel width is swept in the y -direction. Thus, the intensity data in the exposure line is acquired simultaneously, while the acquisition time difference occurs in the different exposure lines. Each data point of the intensity profile of #1 (#2) is obtained by the summation of the photoelectron intensity within a 750 nm window, corresponding to 74 pixels, in the x -(y)-direction. Therefore, the intensity profile of #2 is more affected by the vibration of the instruments than that of #1.

B. Energy resolution

The energy resolution of our spectrometer is evaluated with Au(111). The 10.9-eV laser was used as an excitation source. The measurement was performed with the momentum space mode, and the IDEA was used for the energy filtering. The pass energy of the IDEA was set to 12.5 eV and the slit width to 0.5 mm. The sample temperature was kept at 50 K. Plots in Figure 4 are obtained by integrating the photoelectron intensity in the wavenumber region where the bulk band of Au(111) appears. The intensity plots are fitted with a Fermi-Dirac distribution function convoluted by the Gauss-

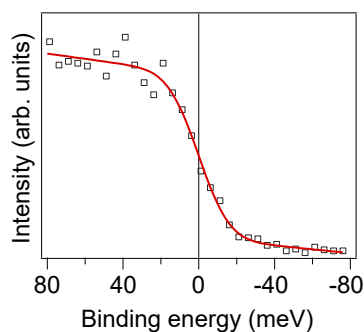


Figure 4: Photoelectron intensity from Au(111) at the Fermi level. The IDEA is used for energy filtering. Square symbols represent the experimental result. The solid curve is a fitting result with the Fermi-Dirac distribution function convoluted by the Gauss-

ian. From the fitting, the energy resolution is estimated to be 24 meV.

IV. DEMONSTRATION

As a demonstration of ARPES measurement with our system, we measured the electronic band structure of Au(111). It is well known that a Shockley-type surface state appears around $\bar{\Gamma}$ in the surface Brillouin zone of Au(111). The surface state exhibits a parabolic energy dispersion with a bottom at a binding energy of 0.48 eV, and the Fermi surface is circular [29]. Besides, the spin degeneracy of the surface state is lifted due to the strong spin-orbit interaction, resulting in the Rashba-type spin-split bands [30]. Spin polarization of the Au(111) surface state has been investigated in detail by SARPES [31]. In addition to Au(111), the spin polarizations of the Shockley-type surface electronic states of Cu(111) and Ag(111) have also been revealed by high-resolution SARPES [32].

A clean surface of Au(111) was obtained by cycles of Ar^+ sputtering and annealing at 550°C. The clean surface was confirmed by observing sharp (1×1) spots and additional satellite spots attributed to the herringbone superstructure on the Au(111) surface by LEED. Photoelectrons were excited by the 10.9-eV laser with a p-polarization, where the electric-field vector of the laser is parallel to the light incident plane. We used the IDEA for the energy analysis of the photoelectron, where the pass energy was 25 eV, and the slit width was 0.5 mm. The FoV in the real space was set to 80 μm . The sample temperature was kept at 30 K during the measurements.

Figure 5(a, b) displays an E - k_x - k_y cube from the lowest cut-off to the highest cut-off energies (i.e., from zero kinetic energy to the Fermi level) and an E - k_x image obtained by slicing the E - k_x - k_y cube at $k_y = 0$, respectively. In our spectrometer, the energy dispersion of the band is obtained as a three-dimensional cube: energy (E), x wavenumber (k_x), and y wavenumber (k_y). Therefore, the band structure of any E - k_{\parallel} cuts of interest can be obtained, as demonstrated in Figure 5(b). A parabolic photoemission horizon with an energy bottom of $E_B = 5.5$ eV is identified. The Shockley-type surface state appears near the Fermi level around $\bar{\Gamma}$, which agrees with the previous report [29]. Several bands attributed to the bulk states are observed in the deeper binding energy side.

The constant energy ARPES intensity image at $E_B = 5.0$ eV is shown in Figure 5(c). The momentum (k) resolution is evaluated from the intensity profile of the edge of the photoemission horizon [Figure 5(d)]. In the fitting procedure, we used the step function convoluted by the Gaussian, as in the case of the spatial-resolution estimation shown in Figure 3(c, d). As a result, the k resolution is estimated to be 0.021 \AA^{-1} .

Figure 5(e) shows the Fermi surface image of Au(111) recorded with the same experimental conditions as in Figure 5(a), but only with improved statistics. A circular-shaped Fermi surface centered at $\bar{\Gamma}$ is observed, attributed to the

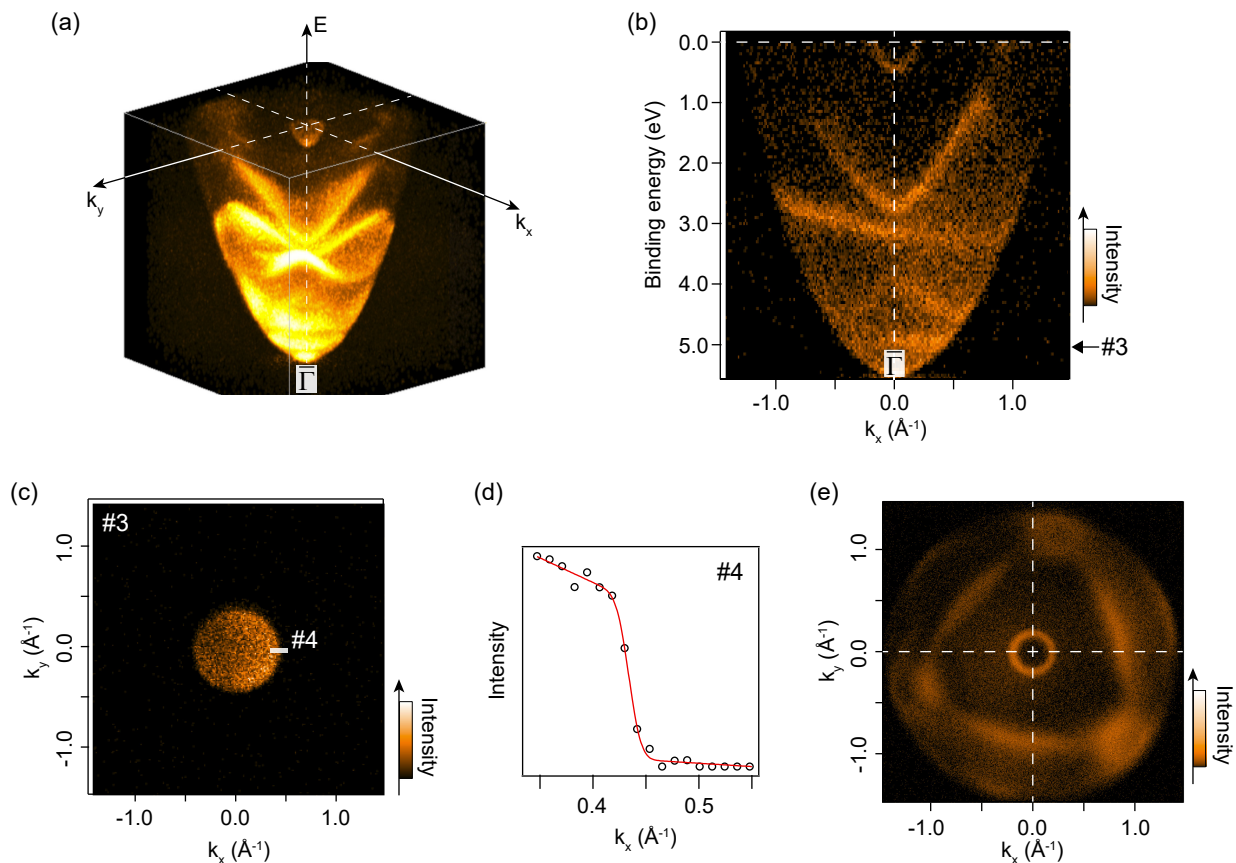


Figure 5: (a) ARPES intensity mapping from Au(111) in the E - k_x - k_y cube. (b) ARPES intensity image obtained by slicing the E - k_x - k_y cube at $k_y = 0$. (c) Constant energy ARPES intensity map in the k_x - k_y plane at #3 shown in (b). (d) Photoelectron intensity plots along #4 shown in (c). Circle symbols represent experimental data. The solid curve gives the fitting result with the step function convoluted by the Gaussian. (e) Constant energy ARPES intensity map in the k_x - k_y plane at the Fermi level.

Shockley-type surface state. In our result, however, no apparent band splitting has been visible. According to the previous study [29, 31], the size of the spin splitting of the surface state for Au(111) is 0.02 \AA^{-1} , which is comparable to or slightly smaller than the k resolution of our spectrometer. Therefore, we could not observe a clear band splitting due to the lack of the k resolution.

V. SUMMARY

A photoemission microscopy apparatus with Nano-ESCA using a 10.9-eV laser has been developed at NIMS. Our apparatus enables energy-filtered photoelectron imaging in both real and momentum spaces. The energy resolution of the spectrometer has been estimated to be 24 meV. In the real (momentum) space mode, the spatial (k) resolution has been 30 nm (0.021 \AA^{-1}). We have performed the ARPES measurements of Au(111) to demonstrate the capability of our apparatus. The high spatial resolution of the machine paves the way for new opportunities, particularly in fields such as submicrometer-scale materials, polycrystals, and combinatorial materials that have yet to be the target of the conventional photoemission spectroscopy.

Acknowledgments

The authors thank Nils Weber for technical support in developing the spectrometer. The present work was partially supported by the Japan Society for the Promotion of Science KAKENHI (Grant Nos. JP21K04633 and JP22H01761), the Innovative Science and Technology Initiative for Security Grant Number JPJ004596, ATLA, Japan, and Iketani Science and Technology Foundation.

References

- [1] S. Hüfner, *Photoelectron Spectroscopy: Principles and Applications* (Springer-Verlag, Berlin, Heidelberg, 2003) Chap. 7.
- [2] P. D. Johnson, *Rep. Prog. Phys.* **60**, 1217 (1997).
- [3] J. A. Sobota, Y. He, and Z.-X. Shen, *Rev. Mod. Phys.* **93**, 025006 (2021).
- [4] L. Mino, E. Borfecchia, J. Segura-Ruiz, C. Giannini, G. Martinez-Criado, and C. Lamberti, *Rev. Mod. Phys.* **90**, 025007 (2018).
- [5] R. Noguchi, T. Takahashi, K. Kuroda, M. Ochi, T. Shirasawa, M. Sakano, C. Bareille, M. Nakayama, M. D. Watson, K. Yaji, A. Harasawa, H. Iwasawa, P. Dudin, T. K. Kim, M. Hoesch, V. Kandyba, A. Giampietri, A. Barinov, S. Shin, R. Arita, T. Sasagawa, and T. Kondo, *Nature* **566**, 518 (2019).
- [6] H. Iwasawa, P. Dudin, K. Inui, T. Masui, T. K. Kim, C. Cacho, and M. Hoesch, *Phys. Rev. B* **99**, 140510(R) (2019).

- [7] P. Dudin, P. Lacovig, C. Fava, E. Nicolini, A. Bianco, G. Cautero, and A. Barinov, *J. Synchrotron Radiat.* **17**, 445 (2010).
- [8] Spatially-resolved angle-resolved photoemission spectroscopy at the Advanced Light Source. <https://sites.google.com/a/lbl.gov/maestro/> (Last accessed: October 1, 2023).
- [9] J. Avila, I. Razado-Colambo, S. Lorcy, B. Lagarde, J.-L. Giorgetta, F. Polack, and M. C. Asensio, *J. Phys. Conf. Ser.* **425**, 192023 (2013).
- [10] M. Hoesch, T. K. Kim, P. Dudin, H. Wang, S. Scott, P. Harris, S. Patel, M. Matthews, D. Hawkins, S. G. Alcock, T. Richter, J. J. Mudd, M. Basham, L. Pratt, P. Leicester, E. C. Longhi, A. Tamai, and F. Baumberger, *Rev. Sci. Instrum.* **88**, 013106 (2017).
- [11] K. Horiba, Y. Nakamura, N. Nagamura, S. Toyoda, H. Kumigashira, M. Oshima, K. Amemiya, Y. Senba, and H. Ohashi, *Rev. Sci. Instrum.* **82**, 113701 (2011).
- [12] M. Escher, N. Weber, M. Merkel, C. Ziethen, P. Bernhard, G. Schönhense, S. Schmidt, F. Forster, F. Reinert, B. Krömker, and D. Funnemann, *J. Phys. Condens. Matter* **17**, S1329 (2005).
- [13] M. Escher, K. Winkler, O. Renault, and N. Barrett, *J. Electron Spectrosc. Relat. Phenom.* **178–179**, 303 (2010).
- [14] M. Patt, C. Wiemann, N. Weber, M. Escher, A. Gloskovskii, W. Drube, M. Merkel, and C. M. Schneider, *Rev. Sci. Instrum.* **85**, 113704 (2014).
- [15] B. Krömker, M. Escher, D. Funnemann, D. Hartung, H. Engelhard, and J. Kirschner, *Rev. Sci. Instrum.* **79**, 053702 (2008).
- [16] C. Tusche, A. Krasnyuk, and J. Kirschner, *Ultramicroscopy* **159**, 520 (2015).
- [17] S. Suga and C. Tusche, *J. Electron Spectrosc. Relat. Phenom.* **200**, 119 (2015).
- [18] C. Tusche, Y.-J. Chen, C. M. Schneider, and J. Kirschner, *Ultramicroscopy* **206**, 112815 (2019).
- [19] C. Tusche, Y.-J. Chen, L. Plucinski, and C. M. Schneider, *e-J. Surf. Sci. Nanotechnol.* **18**, 48 (2020).
- [20] F. Matsui, S. Makita, H. Matsuda, T. Yano, E. Nakamura, K. Tanaka, S. Suga, and S. Kera, *Jpn. J. Appl. Phys.* **59**, 067001 (2020).
- [21] T. Taniuchi, Y. Kotani, and S. Shin, *Rev. Sci. Instrum.* **86**, 023701 (2015).
- [22] J. Madéo, M. K. L. Man, C. Sahoo, M. Campbell, V. Pareek, E. L. Wong, A. Al-Mahboob, N. S. Chan, A. Karmakar, B. M. K. Mariserla, X. Li, T. F. Heinz, T. Cao, and K. M. Dani, *Science* **370**, 1199 (2020).
- [23] O. Karni, E. Barré, V. Pareek, J. D. Georgaras, M. K. L. Man, C. Sahoo, D. R. Bacon, X. Zhu, H. B. Ribeiro, A. L. O’Beirne, J. Hu, A. Al-Mahboob, M. M. M. Abdelrasoul, N. S. Chan, A. Karmakar, A. J. Winchester, B. Kim, K. Watanabe, T. Taniguchi, K. Barmak, J. Madéo, F. H. da Jornada, T. F. Heinz, and K. M. Dani, *Nature* **603**, 247 (2022).
- [24] O. Renault, H. Kim, D. Dumcenco, D. Unuchek, N. Chevalier, M. Gay, A. Kis, and N. Fairley, *J. Vac. Sci. Technol. A* **39**, 053210 (2021).
- [25] Y. He, I. M. Vishik, M. Yi, S. Yang, Z. Liu, J. J. Lee, S. Chen, S. N. Rebec, D. Leuenberger, A. Zong, C. M. Jefferson, R. G. Moore, P. S. Kirchmann, A. J. Merriam, and Z.-X. Shen, *Rev. Sci. Instrum.* **87**, 011301 (2016).
- [26] T. Shimojima, K. Okazaki, and S. Shin, *J. Phys. Soc. Jpn.* **84**, 072001 (2015).
- [27] X. Zhou, S. He, G. Liu, L. Zhao, L. Yu, and W. Zhang, *Rep. Prog. Phys.* **81**, 062101 (2018).
- [28] K. Yaji, A. Harasawa, K. Kuroda, S. Toyohisa, M. Nakayama, Y. Ishida, A. Fukushima, S. Watanabe, C. Chen, F. Komori, and S. Shin, *Rev. Sci. Instrum.* **87**, 053111 (2016).
- [29] F. Reinert, G. Nicolay, S. Schmidt, D. Ehm, and S. Hüfner, *Phys. Rev. B* **63**, 115415 (2001).
- [30] S. LaShell, B. A. McDougall, and E. Jensen, *Phys. Rev. Lett.* **77**, 3419 (1996).
- [31] M. Hoesch, M. Muntwiler, V. N. Petrov, M. Hengsberger, L. Patthey, M. Shi, M. Falub, T. Greber, and J. Osterwalder, *Phys. Rev. B* **69**, 241401(R) (2004).
- [32] K. Yaji, A. Harasawa, K. Kuroda, R. Li, B. Yan, F. Komori, and S. Shin, *Phys. Rev. B* **98**, 041404(R) (2018).



All articles published on e-J. Surf. Sci. Nanotechnol. are licensed under the Creative Commons Attribution 4.0 International (CC BY 4.0). You are free to copy and redistribute articles in any medium or format and also free to remix, transform, and build upon articles for any purpose (including a commercial use) as long as you give appropriate credit to the original source and provide a link to the Creative Commons (CC) license. If you modify the material, you must indicate changes in a proper way.

Copyright: ©2024 The author(s)

Published by The Japan Society of Vacuum and Surface Science